Title: Molecular profiling of primary renal diffuse large B-cell lymphoma unravels a proclivity for immune-privileged organ-tropism

Authors: Axel Künstner[1,2]*, Vera von Kopylow [1,3,4]*, Philipp Lohneis[4]*, Matthias Kümmel[1,3,4], Hanno M. Witte[1,3,5], Lorenz Bastian[1,6], Veronica Bernard[4], Stephanie Stölting[4], Kathrin Kusch[4], Manuela Krokowski[4], Nikolas von Bubnoff[1,3], Konrad Steinestel[7], Annette Arndt[7], Hartmut Merz[4], Hauke Busch[1,2**], Alfred C. Feller[4**], Niklas Gebauer[1,3**]

Affiliations:

[1] University Cancer Center Schleswig-Holstein, University Hospital of Schleswig-Holstein, Campus Lübeck, 23538 Lübeck, Germany

[2] Medical Systems Biology Group, University of Lübeck, Ratzeburger Allee 160, 23538 Lübeck, Germany

[3] Department of Hematology and Oncology, University Hospital of Schleswig-Holstein, Campus Lübeck, Ratzeburger Allee 160, 23538 Lübeck, Germany

[4] Hämatopathologie Lübeck, Reference Centre for Lymph Node Pathology and Hematopathology, Maria-Goeppert-Straße 9a, 23562 Lübeck, Germany.

[5] Department of Hematology and Oncology, Federal Armed Forces Hospital Ulm, Oberer Eselsberg 40, 89081 Ulm

[6] Medical Department II, Hematology and Oncology, University Hospital Schleswig-Holstein, Kiel, Germany.

[7] Department of Pathology, Federal Armed Forces Hospital Ulm, Oberer Eselsberg 40, 89081 Ulm

Running Title: Molecular landscape in primary renal DLBCL

Key Words: PR-DLBCL, molecular landscape, immune-privileged site, MHC Class I and II

Word Count (Abstract): 200

Word Count (Text): 3.782

References: 57

Figures: 6

Supplementary Tables: 8

Supplemental Figures: 4

Supplementary References: 9

Competing Interests: Niklas Gebauer received travel support from Beigene, Janssen, and Roche as well as honoraria from Roche, Takeda, Janssen, Menarini Stemline, and AstraZeneca.

*These authors contributed equally to this manuscript.

**Shared senior authorship

Date of submission: 28.06.2024

Corresponding Author:

PD Dr. med. Niklas Gebauer

Department of Hematology and Oncology

UKSH Campus Luebeck

Ratzenburger Allee 160

23538 Luebeck

Email: Niklas.Gebauer@uksh.de

Abstract:

Primary renal manifestations of diffuse large B-cell lymphoma (PR-DLBCL) represent an exceptionally rare variant of the most common type of non-Hodgkin lymphoma (NHL). Insights into PR-DLBCL pathogenesis have been limited to small case series and methodologically limited approaches. The mechanisms driving lymphomagenesis within an organ lacking an intrinsic lymphatic niche and its proclivity for dissemination to immune-privileged sites, including testes and central nervous system, remain poorly understood. To decode the genetic and transcriptional framework of PR-DLBCL, we utilized whole exome sequencing, array-based somatic copy number alterations analysis, and RNA sequencing. Hereby we characterize the most extensive cohort of PR-DLBCL published, comprising 34 samples from 30 patients. Despite significant mutational heterogeneity with a broad distribution among molecular clusters, we observed a strong unifying enrichment in deleterious MHC class I and II aberrations and loss of *CDKN2A* at a frequency similar to primary large B-cell lymphoma of immune privileged sites (IP-LBCL) alongside significant transcriptional deregulation of interferon signaling and MYC targets in MHC class I-deficient cases.

Our integrative assessment of PR-DLBCL biology expands the molecular understanding of this rare variant including similarities with IP-LBCL as an intriguing explanation for its clinical behavior and tropism. Our observations may inform future risk-adapted therapeutic approaches.

Introduction:

Diffuse large B-cell lymphoma (DLBCL) is the most common type of non-Hodgkin lymphoma (NHL) and accounts for 30 – 40% of newly diagnosed lymphomas [1]. Extranodal manifestations in both the adrenal glands and the kidneys constitute long-standing risk factors for developing simultaneous or secondary CNS manifestations [2]. Secondary renal

involvement is recurrently observed in advanced-stage non-Hodgkin lymphoma (NHL), whereas primary renal (PR-) NHL manifestations are notably less frequent, leading to skepticism regarding the existence of primary renal lymphoma for an extended period [2-6]. Population-based datasets suggest an age-adjusted incidence of 0.035/100,000 with an increasing tendency, a median age of approximately 70 years at diagnosis, a male predominance, and mostly unilateral tumors. Among PR-NHL, DLBCL appears to be the most common histology followed by marginal zone (MZL) and follicular lymphoma (FL) [7, 8]. Clinical differentiation of PR-NHL from other renal malignancies including renal cell carcinoma poses a long-standing challenge, which led to a substantial number of PR-NHL patients undergoing curatively intended resection [9]. In recent years, the introduction of FDG-PET-CTs into routine clinical practice has enabled a more reliable characterization, particularly in patients with more aggressive PR-NHL[10].

Insufficient characterization of pathogenetic mechanisms in indolent PR-DLBCL derives from limited data, primarily comprised of small case series and a lack of in-depth molecular characterization of patients and samples [11]. Molecular drivers of lymphomas originating from organs lacking an intrinsic lymphatic niche, such as the kidney, remain widely elusive apart from individual case studies [12]. To elucidate the genetic and transcriptional landscape and drivers of PR-DLBCL, we conducted a comprehensive investigation employing whole exome sequencing (WES), array-based analysis of somatic copy number alterations (SCNA), and RNA sequencing (RNA-seq) to unravel both molecular properties of this rare entity as well as the cellular composition of its tumor microenvironment (TME).

Materials and methods

Case selection and clinicopathological assessment

For this retrospective analysis, we reviewed our institutional archive for cases of histologically confirmed primary renal DLBCL between January 2001 and December 2021.

Only such cases without concurrent non-renal lymphoma manifestations at diagnosis were included in the study, which led to a large subset of samples obtained by complete renal resection under the suspicion of non-metastatic renal cell carcinoma (22/34 samples; 65%). The study was approved by the ethics committee of the University of Lübeck (reference-no 18-356) and conducted per the declaration of Helsinki. Patients provided written informed consent regarding routine diagnostic and academic assessment, including genomic studies. Histopathological work-up was performed as described and diagnosis was confirmed following the 5th edition WHO classification of hematopoietic and lymphoid tumors and the ICC criteria and yielded 34 cases of PR-DLBCL for which sufficient formalin-fixed paraffin-embedded (FFPE) tissue samples were available for subsequent molecular analysis [1, 13, 14].

Delineation of the molecular composition of the study cohort

Extraction of nucleic acids, WES and RNA-seq alongside detection of Somatic Copy Number Alterations employing the OncoScan CNV array (ThermoFisher was performed as described, and Raw fastq files have been added to the European Genome-phenome archive (EGA) under the previous accession number EGA50000000386 [13, 15]. OncoScan Array data has been deposited in Gene Expression Omnibus (GEO) under accession number GSE270422.

Whole exome data processing and variant calling

The raw sequencing data in FASTQ format was processed using the NFORE workflow (NEXTFLOW v23.10.1) SAREK (v3.3.2) for variant calling against the GRCh38 reference genome [16, 17]. Initially, reads were trimmed for adapter sequences and quality using FASTP (v0.23.4), followed by alignment with BWA MEM2 (v2.2.1) [18, 19]. Subsequent steps included mate-pair information correction, removal of PCR duplicates, and base quality recalibration utilizing PICARD TOOLS, GATK (v4.4.0.0), and dbSNP v146 [20, 21]. Finally, variant calling was executed in tumor-only mode using MUTECT2 with GNOMAD (r2.1.1) as the reference for

known germline variants [22, 23]. Variants were left aligned (GATK LEFTALIGNANDTRIMVARIANTS) and only variants with a PASS filter flag were kept for variant annotation using VARIANT EFFECT PREDICTOR (VEP v111, GRCh38; adding CADD v1.6, dbNSFP v4.1a, and GNOMAD r3.0 as additional annotations) [24-26]. Next, annotations were converted into *MAF* format using VCF2MAF (V1.6.21) (DOI:10.5281/ZENODO.593251); coverage was extracted directly from the vcf INFO field. Potential FFPE artifacts in the variant data were identified using two approaches. First, strand orientation biases (mutations just found on one strand, F1R2 or F2R1) were detected by SOBDETECTOR (v1.0.4) and potential artifacts were removed [27]. Next, a classifier detecting the origin of mutation in formalin-fixation paraffin-embedding (FFPE) samples was applied (R-package EXCERNO v0.1.0) [28]. Variants annotated with an FFPE-like signature were removed. Potential germline variants in the data were removed using GATKs 1000g Panel of Normals. The top 20 frequently mutated genes (FLAGS)[29] were removed from further analysis and the remaining somatic variants were filtered as follows: minimum coverage of 50, minimum alternative allele coverage of 5, minimum variant allele frequency of 10%, and only variants with a frequency < 0.1% in 1000 genomes, GNOMAD, or ExAC were considered for subsequent downstream analysis; variants were required to have a COSMIC or dbSNP ID. High-impact variants (CADD score > 20) in candidate genes (see below) were filtered as such that minimum coverage of 10, minimum alternative coverage of 4, and minimum variant allele frequency of 10% was required. Candidate genes were defined as follows: (a) listed as tumor suppressor or oncogene according to Vogelstein et al. [30], (b) genes from the Lymphgen algorithm, (c) DLBCL genes described by Chapuy *et al.*, (d) MHC genes according to Harmonizome (v3.0) [31-33]. A brief graphical representation of the bioinformatics workflow for WES data processing is provided in **Supplementary Figure S1**.

Detection of Somatic Copy Number Alterations

Somatic copy number alterations were detected using OncoScan CNV assays (ThermoFisher). Raw data (CEL files) were processed using the EACON package (v0.3.6-2) with SEQUENZA as segmentation algorithm [34]. L2R files in CBS format were used as input for GISTIC (v2.0.22) to identify regions significantly amplified or deleted across all samples (confidence level 0.90, focal length cutoff 0.5, q-value threshold 0.1) [34, 35].

For details on transcriptome data quantification, fusion detection, statistical analysis, and pseudonymization, please see **Supplementary Materials and Methods**.

Results

Clinicopathological Characteristics and Cell-of-Origin in PR-DLBCL

We collected 34 PR-DLBCL samples from 30 patients with sufficient FFPE tissue samples for in-depth molecular characterization (**Figure 1A**). The median age of the study group was 66.5 years, 13 patients were female and 17 were male. No iatrogenic immunosuppression, immunodeficiency, and history or current presence of other lymphomas were reported in any of the patients. In particular, only patients without suspicion of concurrent lymphoma manifestations were eligible for the study. This is mirrored in the exceptionally high frequency of cases that underwent surgical resection of the kidney (22/34 cases; 65%). Baseline clinicopathological data are summarized in **Supplementary Table 1**.

Structural variants in *BCL2*, *BCL6*, and *MYC* were assessed successfully in 19, 18, and 17 patients by FISH break-apart probes. In cases without sufficient tissue for FISH but with RNA-seq data, we screened for high-confidence *BCL2/BCL6/MYC* fusions (**Figure 1 B**). Here, we observed aberrations in five (26 %), two (11 %), and three (18%) cases respectively, indicative of a slightly elevated frequency of these aberrations in comparison to DLBCL (NOS) of other primary manifestations. In addition, we observed two cases with ETV6-Ig

fusions, previously described in PCNSL another case of an ETV6:PAX5 fusion respectively, previously described to lead to similar ETV6 activation in B-cell precursor acute lymphoblastic leukemia [36, 37]. Manually curated oncogenic fusions derived from RNA-seq data are summarized in **Supplementary Table 2**. By immunohistochemistry according to the Hans *et al.* algorithm in all samples with sufficient tissue available after DNA/RNA extraction, we observed the majority of cases to be of non-GCB type (18/30; 60%), whereas only a minor subset was of GCB type (11/30; 37%), and one case could not be classified due to insufficient immunoreactivity [38]. Only one case was EBV-associated (>50% positive tumor cells by EBER-ISH). To further unravel the cell of origin, we performed RNA-seq on samples from 30 patients and applied the approach proposed by Wright *et al.* and found 15/30 cases (50%) to be of ABC-subtype. In comparison, 9/30 (30%) were GCB-DLBCL and six remaining cases (20%) remained unclassifiable [31, 39] (**Figure 1 C**).

The mutational landscape of PR-DLBCL

To elucidate the mutational landscape of PR-DLBCL and to screen for mutational drivers of the subgroup's peculiar tropism, we performed WES on FFPE tissue samples from 34 patients (**Figure 1 D**).

Adhering to stringent variant filtering, outlined above, oncogenic mutations were identified in all PR-DLBCL cases. In total 3,178 presumably deleterious mutations, affecting 1,388 genes were observed. Additionally, 25,457 somatic copy number aberrations (SCNAs) were detected. SNVs and indels comprised 11% of these mutations, of which 2,673 were missense (84%), 333 nonsense (10%) and 70 indel mutations (2%). Mutations affecting splice sites represented 3% of estimated somatic mutations and one of the observed mutations was a non-stop mutation (**Supplementary Table 3**). At an intermediate-low median tumor mutational burden (TMB) of 2.45 mutations/Mb (range 0.18 – 5.76), we observed no cases of microsatellite instability as could be expected in aggressive B-cell lymphomas. Variants per

variant class as well as variants per sample including information on variant subtypes are provided in **Supplementary Figure S2**.

The most commonly mutated genes included chromatin-remodeling genes *CREBBP* and *KMT2D* both in 56% of cases with > 20% nonsense mutations, followed by NOTCH signaling-associated genes *SPEN* and *NOTCH2* (both 50%) with nonsense mutations in 47% and 18% respectively. Overall, we observed an enrichment in IL6/JAK/STAT3 signaling mutations including *STAT3*, *PIM1*, and *MYD88*. While *STAT3* mutations were distributed throughout the entire gene, we observed mutational impairment of pre-described hotspots in *MYD88* and *PIM1* (all restricted to the kinase domain) (**Figure 2**). Other biological processes targeted by deleterious mutations in PR-DLBCL included the epigenetic regulation of gene expression (*SF3B1*, *KMT2D*, and *EZH2*), as well as B-cell receptor and RTK-RAS signaling (*CARD11*, *PRDM1*, and *BRAF*). The distribution of mutation onto the candidate driver genes referenced above is displayed in **Figure 2**. In a more global approach, we assessed the impairment of key biological processes through an enrichment analysis of mutations against previously described oncogenetic gene sets and against the IL6/JAK/STAT3 signaling pathway (**Figure 3**) [40]. Hereby we uncovered a relatively wide distribution within a given set (**Figure 3A**). Intriguingly, the most commonly affected gene sets included NOTCH, RTK-RAS, and IL6/JAK/STAT signaling at 97%, 94%, and 91%, respectively (**Figure 3 B, C**). Beyond this, we observed mutational impairment of PI3K signaling in 79% of cases, suggesting a significant role in PR-DLBCL pathogenesis. Correlating information on cell of origin and mutational patterns, we observed a statistically significant enrichment in mutations affecting *TNFAIP3* and *PIM1* among non-GCB cases. *BCL2* rearranged cases showed significantly more *DNMT1* and *SMARCA4* mutations (**Supplementary Figure S3**). We additionally screened for recurrent mutations in canonical tumor suppressor genes (TSGs) and found deleterious mutations in 33/34 (97%) cases. Among the most common targets, in addition to *CREBBP* and *KMT2D*, we observed mutations in *TP53* in 15% of cases.

Genome-wide analysis of somatic copy-number variations in primary renal DLBCL

To unravel the genome-wide landscape of SCNA in PR-DLBCL, we analyzed 29 samples successfully on the Illumina OncoScan array and subsequently employed GISTIC (v2.0.22) to identify regions significantly amplified or deleted across all samples. Arguably the most striking observation was a broad arm-level deletion spanning a large region on chromosome 6 in 48% of evaluable cases (**Figure 4A**). Candidate genes, previously implicated in lymphoma pathogenesis located in this vast region included *PRDM1*, *NFKBIE*, *HLA-A*, *HLA-B*, and *ARID1B*. Beyond this aberration, the genome-wide CNV landscape of PR-DLBCL is dominated by CNVs affecting 3p12.1 and leading to copy number losses of VHL, SETD2, and others (17%), 9p21.3 encompassing the region encoding for TSG *CDKN2A* (38%), as well as the *NOTCH1* region at 9q34.3 (28%). Focal amplifications were observed at 1q23.1, 3p12.3, 3q29, and 22q11.23. Candidate genes among significant deletions and amplifications are provided in **Supplementary Table 4** and **Figure 4B**. To assess the characteristics of PR-DLBCL in contrast to transcriptionally defined subtypes of DLBCL (ABC/GCB) and primary CNS lymphoma (PCNSL) as well as primary testicular large B-cell lymphoma (PTLBL) together representing the subgroup of primary large B-cell lymphomas of immune-privileged sites. We conducted a comparative analysis drawing CNV data from two previously published large-scale genome-wide studies (**Figure 4 C**) [41, 42]. Apart from a focal 3q29 amplification, none of the previously reported copy number gains were observed at a significant level in our cohort. At the same time and of particular interest, we observed strong similarities between PR-DLBCL, PCNSL, and PTLBL regarding deletions at 6p21.33, 6q21, and 6q23.3. Candidate gene deletions previously implicated in post-germinal differentiation and strong CNS tropism located at these loci include *HLA-B* and *PRDM1*. Moreover, we identified the above-mentioned *CDKN2A* deletions in PR-DLBCL at a frequency more similar to PCNSL/PTLBL than an all-comer DLBCL cohort. Additionally, we observed a significant

impact of SCNAs on gene-expression profiles which is shown exemplarily for TSGs (**Supplementary Figure S4**).

Molecular clusters in primary renal DLBCL

Building on our observations from WES, CNV analysis, RNA-seq, alongside structural variants identified by FISH for *BCL2*, *BCL6*, and *MYC*, we performed an integrative analysis on our entire cohort of PR-DLBCL samples to achieve an allocation to the previously defined molecular clusters (A53, N1, BN2, EZB, and MCD) based on the probabilistic LymphGen 2.0 classifier [31]. Molecular data for an integrative analysis of sufficient sensitivity and specificity was available in 30 cases. Unlike previous observations in PCNSL/PTLBL, only one case resembled MCD-DLBCL. The most common molecular subtypes were ST2 (eight cases, 27%) and EZB (five cases, 17%). Of note, no double- or triple-hit lymphomas including MYC+ EZB cases were observed. Only two cases were BN2-DLBCL (7%). While a significant overlap between signatures with compound-cluster allocation was observed in eight cases, six cases were found to exhibit a constellation of findings leading to a classification as “other” (**Figure 1 D** and **Supplementary Table 5**).

Immune-escape mechanisms in primary renal DLBCL as a driver of tropism

Following the characterization of the mutational profiles and molecular clusters that displayed the significant heterogeneity outlined above, we sought to understand the underlying mechanism behind the exceptional renal tropism in our present cohort. Building on our observation of a significant overlap between PR-DLBCL, PCNSL, and PTLBL, in particular regarding copy number losses affecting HLA-B as a hallmark gene of MHC Class I, we sought to assess the extent to which the clinical behavior of PR-DLBCL might be explained by immune escape strategies. Integrating all available datasets, we identified deleterious MHC Class I lesions in 72% of cases, including HLA-A and HLA-B deletions in 48% and

deleterious B2M mutations in 21% of evaluable patients (**Figure 5A, B**). An additional fraction of 33% of patients exhibited deleterious aberrations within the MHC class II machinery and 60% of patients additionally exhibited molecular hits in immediate interaction partners of MHC class I or II required for adequate immune response including del 19p13.3 and mutations affecting CD70, CIITA, and CD58 (**Figure 5A, C**).

Having identified the large-scale 6p25.2-q27 deletion outlined above as a potential hallmark of aggressive B-cell lymphomas with renal tropism, we went on to assess the transcriptional profile of cases carrying said aberration and observed a significantly elevated expression of several candidate genes (**Figure 5D** and **Supplementary Table 6**) including *CXCL10* as well as strong enrichment for interferon alpha and gamma response, MYC targets, JAK/STAT signaling, and others (**Figure 5E** and **Supplementary Table 7**). In particular, we found downstream NFkB activation via TNFalpha signaling. In addition, several metabolic processes including glycolysis, fatty acid metabolism, and oxidative phosphorylation appear to be particularly engaged compared to non-MHC-class I-deleted cases.

Subsequent analysis of our cohort deconvoluting cell states and their assembly into communities of co-association patterns in the form of lymphoma ecotypes (LE) employing the lymphoma EcoTyper revealed a relatively diverse composition of both the tumor as well as its microenvironment in PR-DLBCL [43]. Despite the limited number of cases, we observed a trend towards enrichment in prognostically adverse ABC-DLBCL-associated lymphoma ecotypes (LE) 2 and 4 dominated by B-cells, plasma cells, and dendritic cells as well as NK cells, CD4 and CD8 positive T-cells alongside regulatory T-cells, respectively in del 6p25.2-q27 cases. Moreover, a trend towards enrichment of the T follicular helper cells dominated LE5 was observed in non-del 6p25.2-q27 cases [43]. The distribution of ecotypes on cases is depicted in **Figure 6** (**Supplementary Table 8**).

Discussion

Primary renal DLBCL poses a rare phenomenon associated with adverse clinical features and outcomes, including a so far unexplained CNS tropism leading to significant mortality, especially in relapsed and/or refractory cases [6]. This study was initiated to unravel the molecular underpinnings of primary renal disease, to allow for an understanding as to why and how the disease originates in an organ without a genuine lymphatic niche, and to explain the clinically observed tendency of early CNS progression. To this end, we conducted an integrative analysis employing WES, RNA-seq and array-based SCNV analysis on the largest cohort of PR-DLBCL studied to date.

Hereby, we made the following noteworthy observations. First, we provide a detailed molecular landscape of PR-DLBCL and observe a strong degree of heterogeneity in terms of molecular clusters according to the LymphGen algorithm [31]. Contrary to our initial expectation, we observed a relatively low frequency of *MYD88* mutations. Therefore only one case that was allocated to the characteristic MCD cluster, which is otherwise recurrently observed in both primary and secondary CNS lymphoma as well as testicular lymphoma. Tropism for immune-privileged sites appears to be driven by immune escape strategies, which may be augmented by activating mutations in the B-cell receptor signaling cascade [31, 32, 44, 45]. Beyond this, we saw a high frequency of *SPEN* mutations previously described to be associated with early progression and inferior outcome in an all-comer DLBCL cohort [46]. Significant deregulation of TSGs was further validated via an integrative analysis of SCNAs and transcriptional abundance. Among the genes most commonly affected by mutations within our cohort, potentially targetable vulnerabilities included recurrent mutations in genes like *EZH2* for which clinically active inhibitors have been described previously, including combinations with BCL2 inhibitors in patients with co-occurrence of *EZH2* and *BCL2* aberrations, which we observed in our cohort as well. At the same time, recurrent *CARD11* mutations, downstream of Bruton's tyrosine kinase (BTK) may render therapeutic approaches, employing BTK inhibitors inefficient in a clinically meaningful subset of patients

[47-49]. Given the peculiar tropism of PR-DLBCL, the abundance of *STAT3* mutations appears striking. In addition to the known cooperative interplay between *STAT3* and the NFkB signaling cascade in post-germinal DLBCL, this may further be explained as a selection advantage throughout clonal evolution. In keeping with previous observations that linked *STAT3* mutations and its elevated activity to the modulation of the abundance and function of regulatory T cells in the TME of solid cancers, this suggests a therapeutical perspective involving STAT3 inhibition which might be able to target the TME and its permissive impact on the immunological niche in PR-DLBCL [50, 51]. An additional candidate driver for early progression and CNS dissemination is the relatively high rate of *MYC* aberrations in more than 17% of evaluable cases [52].

Second, we describe a profile of SCNA and mutations leading to significant impairment of MHC class I/II families and its immediately associated genes in approx. 95% of cases in the cohort, which significantly exceeds observations in all-comer DLBCL cohorts [32, 53]. From these observations, we deduce a strong overlap between PR-DLBCL and large B-cell lymphomas of immune-privileged sites (IP-LBCL) regarding SCNAs. At the same time, PR-DLBCL apparently lacks the characteristic mutational profile resulting in tonic B-cell receptor signaling usually associated with this newly described entity [1, 54]. It is tempting to speculate on a theory of a first and second hit in the central nervous dissemination of PR-DLBCL acquiring the typical driver mutations in a second step, following the initial presence of strong immune-escape mechanisms [55]. To investigate this in future studies, paired analyses of renal and CNS tumors will be required. Deleterious aberrations in MHC class I components and related genes constitute well-documented phenomena in DLBCL. However, the frequency at which this is observed in the present study, extending to highly recurrent alterations of MHC class II genes poses a significant enrichment [32]. Moreover, this aligns with previous observations in primary CNS lymphoma and testicular lymphoma regarding deletions of the *HLA* and *CDKN2A* loci and extends well beyond previous reports in ABC-

DLBCL by both immunohistochemistry and gene expression profiling [41]. Further in keeping with pathogenetically similar trajectories between PR-DLBCL and other IP-LBCL, we observed 10% of cases harboring *ETV6* rearrangements previously reported as recurrent, oncogenic structural variants and drivers of a post-germinal phenotype in PCNSL [36].

Third, we describe a characteristic transcriptional profile in cases harboring MHC class I SCNAs as a newly described hallmark of primary renal DLBCL. It is predominantly characterized by a strong enrichment for interferon alpha and gamma responses, MYC targets, and JAK/STAT signaling and downstream NFkB activation via TNF-alpha signaling. All of these mechanisms are known drivers, especially of ABC-DLBCL. TNF signaling was recently shown to aberrantly remodel the fibroblastic reticular cell (FRC) network and contribute to a tolerogenic TME hindering therapeutic efficacy of immune-based therapies [51, 56]. Further, several metabolic processes including glycolysis, fatty acid metabolism, and oxidative phosphorylation appear particularly engaged. This could be particularly interesting in future targeted therapeutical approaches exploiting this dependence, as recently described [57]. In addition, we observed a trend towards enrichment of LE2- and LE4-high states in our predominantly ABC-like group of MHC class I deleted tumors, in keeping with previous observations from all-comer DLBCL cohorts where these lymphoma ecotypes were associated with inferior clinical outcomes [43]. The trend towards more LE5-high tumors in the non-MHC class I deleted cases with its underlying cell states being more prevalent in healthy lymphoid tissues integrates seamlessly with this notion.

The study presents several limitations, inherent to the retrospective design. Despite this being the largest cohort of PR-DLBCL to date the sample size remains limited and samples for the study were collected over more than two decades. This results in significant heterogeneity in terms of first- and later-line treatment approaches and limited follow-up information. These factors prohibit a meaningful integrative analysis of molecular findings and clinical endpoints. In addition, there is a potential for cases with occult non-renal primary

manifestations, which may have been missed by diagnosing physicians. However, considering that secondary renal manifestations typically occur in advanced-stage disease, the likelihood of a significant fraction of patients harboring secondary renal manifestations is relatively low.

In summary, we present the largest molecular study on PR-DLBCL to date, untangle the genomic and transcriptional heterogeneity of the disease, and uncover evidence of significant pathogenetic overlap between PR-DLBCL and IP-LBCL. Our observations may inform future risk-adapted therapeutic approaches.

Declarations

Ethics approval and consent to participate

This retrospective study was approved by the ethics committee of the University of Lübeck (reference-no 18-356) and conducted in accordance with the declaration of Helsinki. Patients have provided written informed consent regarding routine diagnostic and academic assessment, including genomic studies of their biopsy specimens alongside the transfer of their clinical data.

Availability of data and material

Raw fastq files have been deposited in the European genome-phenome archive (EGA) under the accession number EGA50000000386. OncoScan Array data has been deposited in Gene Expression Omnibus (GEO) under accession number GSE270422.

Funding

This work was supported by generous funding by the Wilhelm Sander-Stiftung through a project grant (NG; Grant-Nr.: 2021.150.1). HB and AK acknowledge support from the BMBF project OUTLIVE-CRC (FKZ 01KD2103A).

Author contributions

Study concept: NG, ACF, HM

Data collection: NG, AK, VvK, PL, MK, HW, VB, SS, KK, HM, SS, KS, AA, ACF

Data analysis and creation of figures and tables: AK, NG, ACF, HB, NvB,

Initial Draft of manuscript: NG.

Critical revision and approval of final version: all authors.

Acknowledgements

The authors would like to thank Tanja Oeltermann for her skilled technical assistance. AK and HB acknowledge computational support from the OMICS compute cluster at the University of Lübeck.

References

1. Alaggio R, Amador C, Anagnostopoulos I, Attygalle AD, Araujo IBO, Berti E, *et al.* The 5th edition of the World Health Organization Classification of Haematolymphoid Tumours: Lymphoid Neoplasms. *Leukemia* 2022 Jul; **36**(7)**:** 1720-1748.

2. Schmitz N, Zeynalova S, Nickelsen M, Kansara R, Villa D, Sehn LH, *et al.* CNS International Prognostic Index: A Risk Model for CNS Relapse in Patients With Diffuse Large B-Cell Lymphoma Treated With R-CHOP. *J Clin Oncol* 2016 Sep 10; **34**(26)**:** 3150-3156.

3. Hu R, Zhang R, Miao M, Zhu K, Yang W, Liu Z. Central nervous system involvement of primary renal lymphoma with diffuse large B-cell type lymphoma. *Am J Case Rep* 2013; **14:** 292-294.

4. Gibson TE. Lymphosarcoma of the kidney. *J Urol* 1948 Dec; **60**(6)**:** 838-854.

5. Kandel LB, McCullough DL, Harrison LH, Woodruff RD, Ahl ET, Jr., Munitz HA. Primary renal lymphoma. Does it exist? *Cancer* 1987 Aug 1; **60**(3)**:** 386-391.

6. Okuno SH, Hoyer JD, Ristow K, Witzig TE. Primary renal non-Hodgkin's lymphoma. An unusual extranodal site. *Cancer* 1995 May 1; **75**(9)**:** 2258-2261.

7. Taneja A, Kumar V, Chandra AB. Primary renal lymphoma: A population-based analysis using the SEER program (1973-2015). *Eur J Haematol* 2020 May; **104**(5)**:** 390-399.

8. Chen J, Peng J, Zheng Y, Li S, Yang P, Wu X, *et al.* Primary renal lymphoma: a population-based study in the United States, 1980-2013. *Sci Rep* 2019 Oct 22; **9**(1)**:** 15125.

9. Chen X, Hu D, Fang L, Chen Y, Che X, Tao J, *et al.* Primary renal lymphoma: A case report and literature review. *Oncol Lett* 2016 Nov; **12**(5)**:** 4001-4008.

10. Nicolau C, Sala E, Kumar A, Goldman DA, Schoder H, Hricak H, *et al.* Renal Masses Detected on FDG PET/CT in Patients With Lymphoma: Imaging Features Differentiating

Primary Renal Cell Carcinomas From Renal Lymphomatous Involvement. *AJR Am J Roentgenol* 2017 Apr; **208**(4)**:** 849-853.

11. Garcia M, Konoplev S, Morosan C, Abruzzo LV, Bueso-Ramos CE, Medeiros LJ. MALT lymphoma involving the kidney: a report of 10 cases and review of the literature. *Am J Clin Pathol* 2007 Sep; **128**(3)**:** 464-473.

12. Wen S, Liu T, Zhang H, Zhou X, Jin H, Sun M, *et al.* Whole-Exome Sequencing Reveals New Potential Mutations Genes for Primary Mucosa-Associated Lymphoid Tissue Lymphoma Arising From the Kidney. *Front Oncol* 2020; **10:** 609839.

13. Künstner A, Schwarting J, Witte HM, Bernard V, Stölting S, Kusch K, *et al.* Integrative molecular profiling identifies two molecularly and clinically distinct subtypes of blastic plasmacytoid dendritic cell neoplasm. *Blood Cancer Journal* 2022 2022/07/04; **12**(7)**:** 101.

14. Campo E, Jaffe ES, Cook JR, Quintanilla-Martinez L, Swerdlow SH, Anderson KC, *et al.* The International Consensus Classification of Mature Lymphoid Neoplasms: a report from the Clinical Advisory Committee. *Blood* 2022 Sep 15; **140**(11)**:** 1229-1253.

15. Witte HM, Kunstner A, Hertel N, Bernd HW, Bernard V, Stolting S, *et al.* Integrative genomic and transcriptomic analysis in plasmablastic lymphoma identifies disruption of key regulatory pathways. *Blood Adv* 2021 Oct 29.

16. Ewels PA, Peltzer A, Fillinger S, Patel H, Alneberg J, Wilm A, *et al.* The nf-core framework for community-curated bioinformatics pipelines. *Nat Biotechnol* 2020 Mar; **38**(3)**:** 276-278.

17. Hanssen F, Garcia MU, Folkersen L, Pedersen AS, Lescai F, Jodoin S, *et al.* Scalable and efficient DNA sequencing analysis on different compute infrastructures aiding variant discovery. *NAR Genom Bioinform* 2024 Jun; **6**(2)**:** lqae031.

18. Chen S, Zhou Y, Chen Y, Gu J. fastp: an ultra-fast all-in-one FASTQ preprocessor. *Bioinformatics* 2018 Sep 1; **34**(17)**:** i884-i890.

19. Vasimuddin M, Misra S, Li H, Aluru S. Efficient Architecture-Aware Acceleration of BWA-MEM for Multicore Systems. *2019 IEEE International Parallel and Distributed Processing Symposium (IPDPS)* 2019**:** 314-324.

20. McKenna A, Hanna M, Banks E, Sivachenko A, Cibulskis K, Kernytsky A, *et al.* The Genome Analysis Toolkit: a MapReduce framework for analyzing next-generation DNA sequencing data. *Genome Res* 2010 Sep; **20**(9)**:** 1297-1303.

21. Sherry ST, Ward MH, Kholodov M, Baker J, Phan L, Smigielski EM, *et al.* dbSNP: the NCBI database of genetic variation. *Nucleic Acids Res* 2001 Jan 1; **29**(1)**:** 308-311.

22. Cibulskis K, Lawrence MS, Carter SL, Sivachenko A, Jaffe D, Sougnez C, *et al.* Sensitive detection of somatic point mutations in impure and heterogeneous cancer samples. *Nat Biotechnol* 2013 Mar; **31**(3)**:** 213-219.

23. Karczewski KJ, Francioli LC, Tiao G, Cummings BB, Alfoldi J, Wang Q, *et al.* The mutational constraint spectrum quantified from variation in 141,456 humans. *Nature* 2020 May; **581**(7809)**:** 434-443.

24. McLaren W, Gil L, Hunt SE, Riat HS, Ritchie GR, Thormann A, *et al.* The Ensembl Variant Effect Predictor. *Genome Biol* 2016 Jun 6; **17**(1)**:** 122.

25. Rentzsch P, Witten D, Cooper GM, Shendure J, Kircher M. CADD: predicting the deleteriousness of variants throughout the human genome. *Nucleic Acids Res* 2019 Jan 8; **47**(D1)**:** D886-D894.

26. Chen S, Francioli LC, Goodrich JK, Collins RL, Kanai M, Wang Q, *et al.* A genomic mutational constraint map using variation in 76,156 human genomes. *Nature* 2024 Jan; **625**(7993)**:** 92-100.

27. Diossy M, Sztupinszki Z, Krzystanek M, Borcsok J, Eklund AC, Csabai I, *et al.* Strand Orientation Bias Detector to determine the probability of FFPE sequencing artifacts. *Brief Bioinform* 2021 Nov 5; **22**(6).

28. Mitchell A, Ruiz M, Yang S, Wang C, Davila JI. Excerno: Using Mutational Signatures in Sequencing Data to Filter False Variants Caused by Clinical Archival. *J Comput Biol* 2023 Apr; **30**(4)**:** 366-375.

29. Shyr C, Tarailo-Graovac M, Gottlieb M, Lee JJ, van Karnebeek C, Wasserman WW. FLAGS, frequently mutated genes in public exomes. *BMC Med Genomics* 2014 Dec 3; **7:** 64.

30. Vogelstein B, Papadopoulos N, Velculescu VE, Zhou S, Diaz LA, Jr., Kinzler KW. Cancer genome landscapes. *Science* 2013 Mar 29; **339**(6127)**:** 1546-1558.

31. Wright GW, Huang DW, Phelan JD, Coulibaly ZA, Roulland S, Young RM, *et al.* A Probabilistic Classification Tool for Genetic Subtypes of Diffuse Large B Cell Lymphoma with Therapeutic Implications. *Cancer Cell* 2020 Apr 13; **37**(4)**:** 551-568 e514.

32. Chapuy B, Stewart C, Dunford AJ, Kim J, Kamburov A, Redd RA, *et al.* Molecular subtypes of diffuse large B cell lymphoma are associated with distinct pathogenic mechanisms and outcomes. *Nat Med* 2018 May; **24**(5)**:** 679-690.

33. Rouillard AD, Gundersen GW, Fernandez NF, Wang Z, Monteiro CD, McDermott MG, *et al.* The harmonizome: a collection of processed datasets gathered to serve and mine knowledge about genes and proteins. *Database (Oxford)* 2016; **2016**.

34. Favero F, Joshi T, Marquard AM, Birkbak NJ, Krzystanek M, Li Q, *et al.* Sequenza: allele-specific copy number and mutation profiles from tumor sequencing data. *Ann Oncol* 2015 Jan; **26**(1)**:** 64-70.

35. Mermel CH, Schumacher SE, Hill B, Meyerson ML, Beroukhim R, Getz G. GISTIC2.0 facilitates sensitive and confident localization of the targets of focal somatic copy-number alteration in human cancers. *Genome Biol* 2011; **12**(4)**:** R41.

36. Bruno A, Labreche K, Daniau M, Boisselier B, Gauchotte G, Royer-Perron L, *et al.* Identification of novel recurrent ETV6-IgH fusions in primary central nervous system lymphoma. *Neuro Oncol* 2018 Jul 5; **20**(8)**:** 1092-1100.

37. Smeenk L, Fischer M, Jurado S, Jaritz M, Azaryan A, Werner B, *et al.* Molecular role of the PAX5-ETV6 oncoprotein in promoting B-cell acute lymphoblastic leukemia. *EMBO J* 2017 Mar 15; **36**(6)**:** 718-735.

38. Hans CP, Weisenburger DD, Greiner TC, Gascoyne RD, Delabie J, Ott G, *et al.* Confirmation of the molecular classification of diffuse large B-cell lymphoma by immunohistochemistry using a tissue microarray. *Blood* 2004 Jan 1; **103**(1)**:** 275-282.

39. Wright G, Tan B, Rosenwald A, Hurt EH, Wiestner A, Staudt LM. A gene expression-based method to diagnose clinically distinct subgroups of diffuse large B cell lymphoma. *Proc Natl Acad Sci U S A* 2003 Aug 19; **100**(17)**:** 9991-9996.

40. Sanchez-Vega F, Mina M, Armenia J, Chatila WK, Luna A, La KC, *et al.* Oncogenic Signaling Pathways in The Cancer Genome Atlas. *Cell* 2018 Apr 5; **173**(2)**:** 321-337 e310.

41. Chapuy B, Roemer MG, Stewart C, Tan Y, Abo RP, Zhang L, *et al.* Targetable genetic features of primary testicular and primary central nervous system lymphomas. *Blood* 2016 Feb 18; **127**(7)**:** 869-881.

42. Monti S, Chapuy B, Takeyama K, Rodig SJ, Hao Y, Yeda KT, *et al.* Integrative analysis reveals an outcome-associated and targetable pattern of p53 and cell cycle deregulation in diffuse large B cell lymphoma. *Cancer Cell* 2012 Sep 11; **22**(3)**:** 359-372.

43. Steen CB, Luca BA, Esfahani MS, Azizi A, Sworder BJ, Nabet BY, *et al.* The landscape of tumor cell states and ecosystems in diffuse large B cell lymphoma. *Cancer Cell* 2021 Oct 11; **39**(10)**:** 1422-1437 e1410.

44. Wright GW, Wilson WH, Staudt LM. Genetics of Diffuse Large B-Cell Lymphoma. *N Engl J Med* 2018 Aug 2; **379**(5)**:** 493-494.

45. Radke J, Ishaque N, Koll R, Gu Z, Schumann E, Sieverling L, *et al.* The genomic and transcriptional landscape of primary central nervous system lymphoma. *Nat Commun* 2022 May 10; **13**(1)**:** 2558.

46. Ren W, Wan H, Own SA, Berglund M, Wang X, Yang M, *et al.* Genetic and transcriptomic analyses of diffuse large B-cell lymphoma patients with poor outcomes within two years of diagnosis. *Leukemia* 2024 Mar; **38**(3)**:** 610-620.

47. Caeser R, Walker I, Gao J, Shah N, Rasso-Barnett L, Anand S, *et al.* Acquired CARD11 mutation promotes BCR independence in Diffuse Large B Cell Lymphoma. *JCO Precis Oncol* 2021; **5:** 145-152.

48. Scholze H, Stephenson RE, Reynolds R, Shah S, Puri R, Butler SD, *et al.* Combined EZH2 and Bcl-2 inhibitors as precision therapy for genetically defined DLBCL subtypes. *Blood Adv* 2020 Oct 27; **4**(20)**:** 5226-5231.

49. Morschhauser F, Salles G, Batlevi CL, Tilly H, Chaidos A, Phillips T, *et al.* Taking the EZ way: Targeting enhancer of zeste homolog 2 in B-cell lymphomas. *Blood Rev* 2022 Nov; **56:** 100988.

50. Oweida AJ, Darragh L, Phan A, Binder D, Bhatia S, Mueller A, *et al.* STAT3 Modulation of Regulatory T Cells in Response to Radiation Therapy in Head and Neck Cancer. *J Natl Cancer Inst* 2019 Dec 1; **111**(12)**:** 1339-1349.

51. Lam LT, Wright G, Davis RE, Lenz G, Farinha P, Dang L, *et al.* Cooperative signaling through the signal transducer and activator of transcription 3 and nuclear factor-kappaB pathways in subtypes of diffuse large B-cell lymphoma. *Blood* 2008 Apr 1; **111**(7)**:** 3701-3713.

52. Rosenwald A, Bens S, Advani R, Barrans S, Copie-Bergman C, Elsensohn MH, *et al.* Prognostic Significance of MYC Rearrangement and Translocation Partner in Diffuse Large B-Cell Lymphoma: A Study by the Lunenburg Lymphoma Biomarker Consortium. *J Clin Oncol* 2019 Dec 10; **37**(35)**:** 3359-3368.

53. Schmitz R, Wright GW, Huang DW, Johnson CA, Phelan JD, Wang JQ, *et al.* Genetics and Pathogenesis of Diffuse Large B-Cell Lymphoma. *N Engl J Med* 2018 Apr 12; **378**(15)**:** 1396-1407.

54. Roschewski M, Phelan JD, Jaffe ES. Primary Large B-cell Lymphomas of Immune-Privileged Sites. *Blood* 2024 Apr 18.

55. Watanabe J, Natsumeda M, Okada M, Kobayashi D, Kanemaru Y, Tsukamoto Y, *et al.* High Detection Rate of MYD88 Mutations in Cerebrospinal Fluid From Patients With CNS Lymphomas. *JCO Precis Oncol* 2019 Dec; **3:** 1-13.

56. Apollonio B, Spada F, Petrov N, Cozzetto D, Papazoglou D, Jarvis P, *et al.* Tumor-activated lymph node fibroblasts suppress T cell function in diffuse large B cell lymphoma. *J Clin Invest* 2023 Jul 3; **133**(13).

57. Noble RA, Thomas H, Zhao Y, Herendi L, Howarth R, Dragoni I, *et al.* Simultaneous targeting of glycolysis and oxidative phosphorylation as a therapeutic strategy to treat diffuse large B-cell lymphoma. *Br J Cancer* 2022 Sep; **127**(5)**:** 937-947.

Figure Legends:

Figure 1. Molecular landscape of PR- DLBCL. A Venn diagram depicting the number of samples for which WES (n = 34), RNA-seq (n = 30), and OncoScan arrays (n = 29) were successfully conducted. **B** Fusion identified by RNA-sequencing in PR-DLBCL samples (beyond *MYC*/*BCL2*/*BCL6* rearrangements identified in cases studied by FISH) displayed by their genomic location. **C** Sankey plot illustrating the distribution of cases of PR-DLBCL into the categories GCB/non-GCB by immunohistochemistry (IHC) according to the algorithm proposed by Hans *et al.*[38] as well as by Cell-of-origin (CoO) classified according to gene-expression profiling [39] derived from RNA-seq and lastly according to molecular clusters drawn from the LymphGen algorithm, integrating data from WES, RNA-seq, Oncoscans, and FISH (*BCL2*/*BCL6*/*MYC*) [31], depicting the significant degree of molecular heterogeneity. **D** Oncoplot displaying putative driver genes and the number of samples harboring mutations in a given gene (right bar). Mutation types are color-coded, and covariates, including sex, CoO, FISH results for BCL2/BCL6/MYC, and type of biopsy (punch/needle core vs. open resection/nephrectomy) are shown below for each sample.

Figure 2. Recurrently mutated putative drivers of PR-DLBCL. Lollipop plots illustrating types and location of mutations, grouped by affected signaling pathway and/or biological function. Functional domains are depicted as a frame of reference and the lollipops' height indicates the frequency with which a given mutation occurred in our cohort.

Figure 3. Functional implication of mutations in PR-DLBCL. A Fraction of a given pathway, biological function, or gene set impaired by mutations is depicted as the number of affected genes vs. the number of genes in a given set. **B** Distribution of mutational impairment of gene sets per sample, including fraction of samples harboring one or more mutations in a given gene set.

Figure 4. Somatic copy-number aberrations in PR-DLBCL compared with other subtypes of DLBCL including IP-LBCL. A Location of SCNAs along the genome and GISTIC G-scores (G =

Frequency × Amplitude; red bars denote gains and blue bars losses; gene names refer to affected oncogenes and tumor suppressor genes within identified regions). **B** Tumor suppressor genes affected by copy number losses. **C** Amplifications and deletions at recurrently affected loci in an all-comer cohort of DLBCL (first column), DLBCL of ABC- as well as GCB-subtype (second and third column) and IP-LBCL with primary CNS or primary testicular manifestation (column four and five) compared to primary renal DLBCL (column six).

Figure 5. Immune escape is the predominant molecular feature of PR-DLBCL. A Impairment of the MHC class I and II apparatus as well as its immediate interaction partners by mutations and/or SCNAs. **B, C** Lollipop plots illustrating types and location of mutations in *B2M* and *CIITA* as recurrently mutated genes associated with immune escape in PR-DLBCL. Functional domains are depicted as a frame of reference and the lollipops' height indicates the frequency with which a given mutation occurred in our cohort. **D** Volcano plot illustrating results of a genome-wide screen for significantly deregulated genes by the presence or absence of a large-scale deletion on chromosome 6 leading to strong MHC class I impairment as the most recurrent and striking feature in PR-DLBCL. **E** Gene-set enrichment analysis depicting functional implications of deregulated gene expression between cases with and without large-scale MHC class I deletions.

Figure 6. Deconvolution of PR- DLBCL transcriptomes employing the lymphoma EcoTyper. A Heatmap displaying the cell-type abundance as well as the predominant EcoType for a given PR-DLBCL sample. **B** Comparative analysis of lymphoma EcoType abundances according to the presence or absence of a large-scale deletion on chromosome 6 leading to strong MHC class I impairment as the most recurrent and striking feature in prDLBC, grouped by lymphoma EcoTypes.

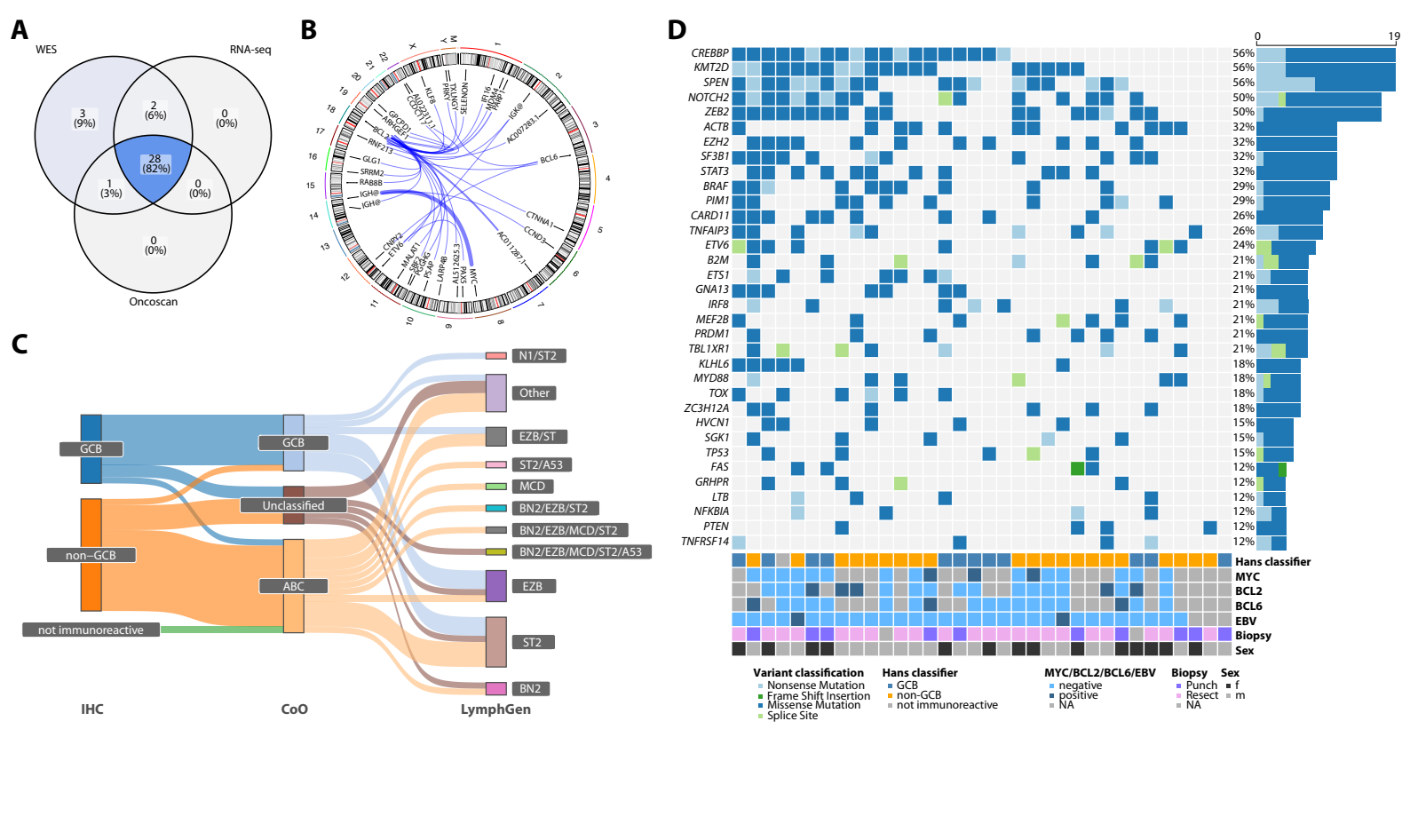
A
WES
RNA-seq
Oncoscan
3 (9%)
2 (6%)
0 (0%)
28 (82%)
1 (3%)
0 (0%)
0 (0%)
B
C
GCB
non–GCB
not immunoreactive
GCB
Unclassified
ABC
N1/ST2
Other
EZB/ST
ST2/A53
MCD
BN2/EZB/ST2
BN2/EZB/MCD/ST2
BN2/EZB/MCD/ST2/A53
EZB
ST2
BN2
IHC
CoO
LymphGen
D
CREBBP
KMT2D
SPEN
NOTCH2
ZEB2
ACTB
EZH2
SF3B1
STAT3
BRAF
PIM1
CARD11
TNFAIP3
ETV6
B2M
ETS1
GNA13
IRF8
MEF2B
PRDM1
TBL1XR1
KLHL6
MYD88
TOX
ZC3H12A
HVCN1
SGK1
TP53
FAS
GRHPR
LTB
NFKBIA
PTEN
TNFRSF14
56%
56%
56%
50%
50%
32%
32%
32%
32%
29%
29%
26%
26%
24%
21%
21%
21%
21%
21%
21%
18%
18%
18%
18%
15%
15%
15%
12%
12%
12%
12%
12%
12%
0
19
Hans classifier
MYC
BCL2
BCL6
EBV
Biopsy
Sex
Variant classification
Nonsense Mutation
Frame Shift Insertion
Missense Mutation
Splice Site
Hans classifier
GCB
non-GCB
not immunoreactive
MYC/BCL2/BCL6/EBV
negative
positive
NA
Biopsy
Punch
Resect
NA
Sex
f
m

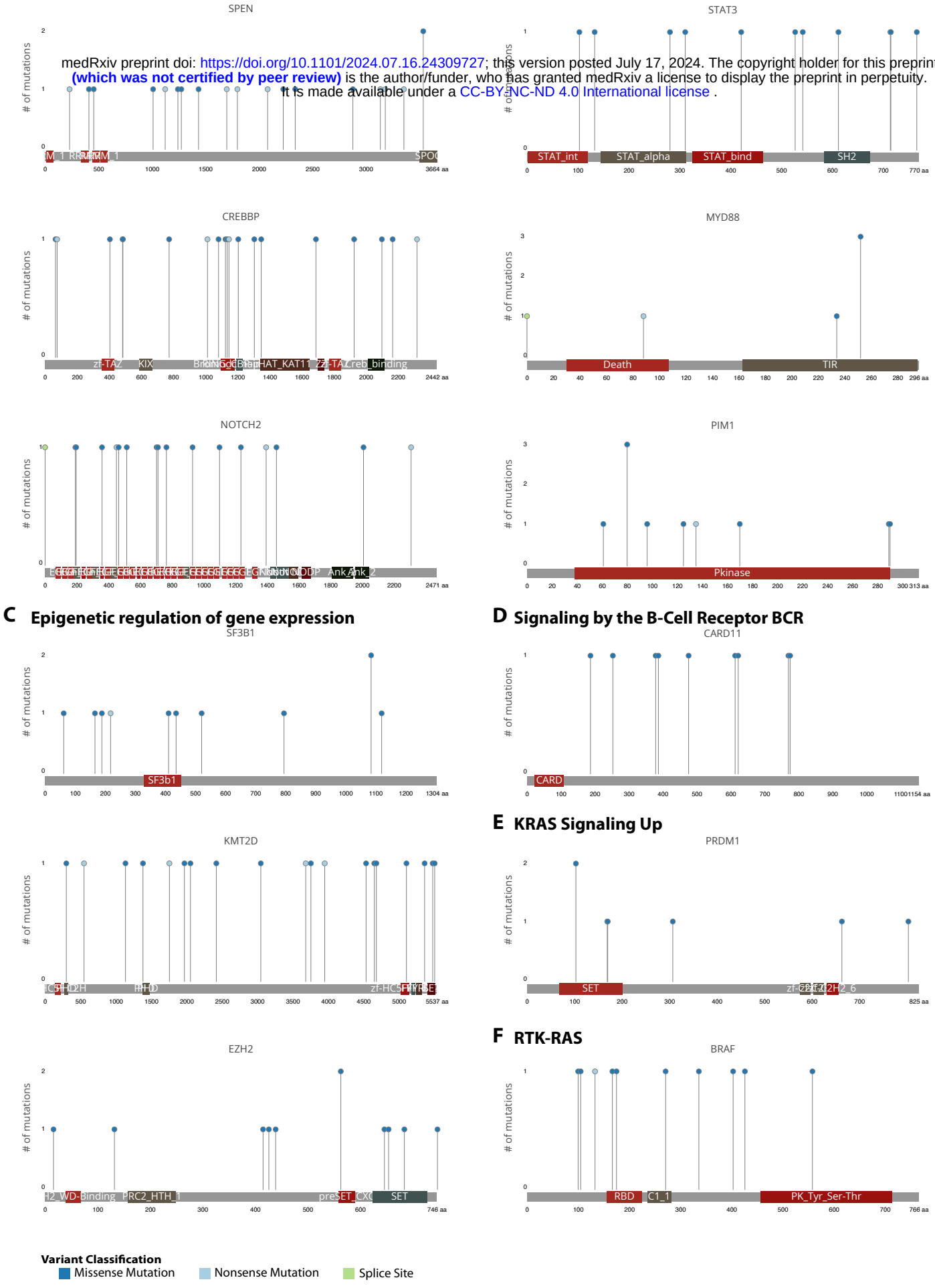

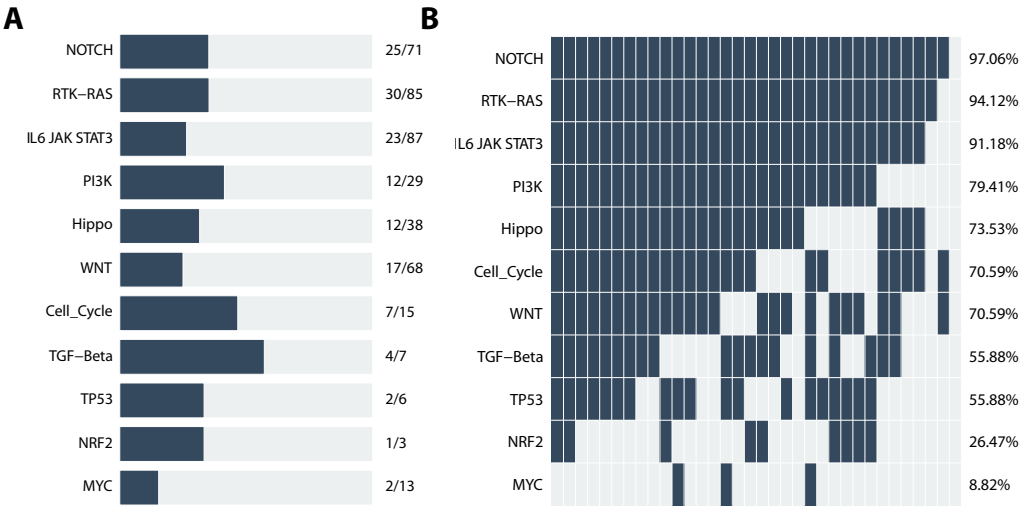
A
NOTCH
RTK−RAS
IL6 JAK STAT3
PI3K
Hippo
WNT
Cell_Cycle
TGF−Beta
TP53
NRF2
MYC
25/71
30/85
23/87
12/29
12/38
17/68
7/15
4/7
2/6
1/3
2/13
0.00
0.25
0.50
0.75
1.00
B
NOTCH
RTK−RAS
IL6 JAK STAT3
PI3K
Hippo
Cell_Cycle
WNT
TGF−Beta
TP53
NRF2
MYC
97.06%
94.12%
91.18%
79.41%
73.53%
70.59%
70.59%
55.88%
55.88%
26.47%
8.82%

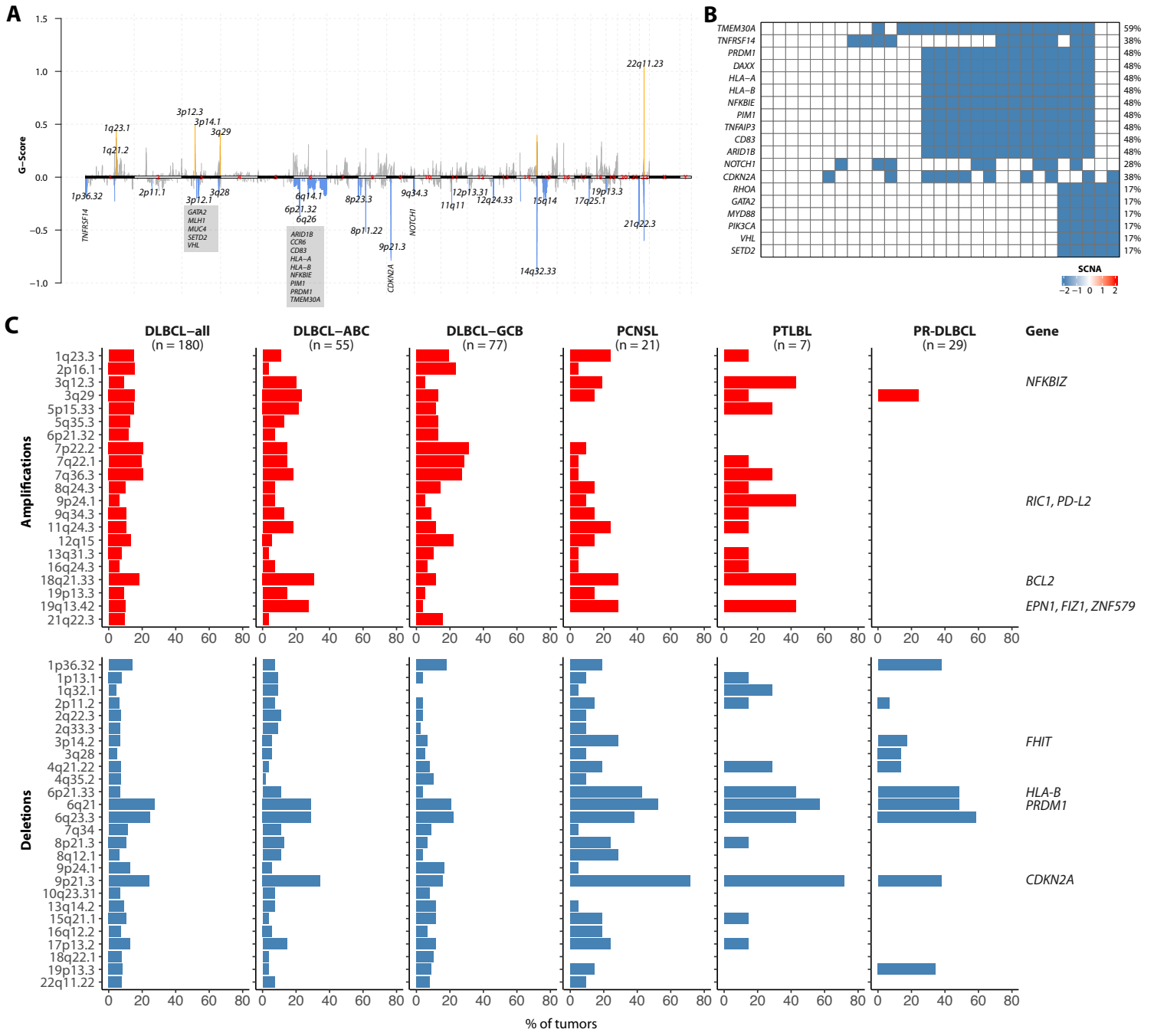
A
G-Score
1.5
1.0
0.5
0.0
−0.5
−1.0
1p36.32
1q23.1
1q21.2
2p11.1
3p12.3
3p14.1
3q29
3p12.1
3q28
6q14.1
6p21.32
6q26
8p23.3
8p11.22
9p21.3
9q34.3
CDKN2A
NOTCH1
11q11
12p13.31
12q24.33
15q14
14q32.33
17q25.1
19p13.3
21q22.3
22q11.23
TNFRSF14
GATA2
MLH1
MUC4
SETD2
VHL
ARID1B
CCR6
CD83
HLA−A
HLA−B
NFKBIE
PIM1
PRDM1
TMEM30A
B
TMEM30A 59%
TNFRSF14 38%
PRDM1 48%
DAXX 48%
HLA−A 48%
HLA−B 48%
NFKBIE 48%
PIM1 48%
TNFAIP3 48%
CD83 48%
ARID1B 48%
NOTCH1 28%
CDKN2A 38%
RHOA 17%
GATA2 17%
MYD88 17%
PIK3CA 17%
VHL 17%
SETD2 17%
SCNA
−2 −1 0 1 2
C
DLBCL−all (n = 180)
DLBCL−ABC (n = 55)
DLBCL−GCB (n = 77)
PCNSL (n = 21)
PTLBL (n = 7)
PR-DLBCL (n = 29)
Gene
Amplifications
1q23.3
2p16.1
3q12.3
3q29
5p15.33
5q35.3
6p21.32
7p22.2
7q22.1
7q36.3
8q24.3
9p24.1
9q34.3
11q24.3
12q15
13q31.3
16q24.3
18q21.33
19p13.3
19q13.42
21q22.3
NFKBIZ
RIC1, PD-L2
BCL2
EPN1, FIZ1, ZNF579
Deletions
1p36.32
1p13.1
1q32.1
2p11.2
2q22.3
2q33.3
3p14.2
3q28
4q21.22
4q35.2
6p21.33
6q21
6q23.3
7q34
8p21.3
8q12.1
9p24.1
9p21.3
10q23.31
13q14.2
15q21.1
16q12.2
17p13.2
18q22.1
19p13.3
22q11.22
FHIT
HLA-B
PRDM1
CDKN2A
0 20 40 60 80
% of tumors

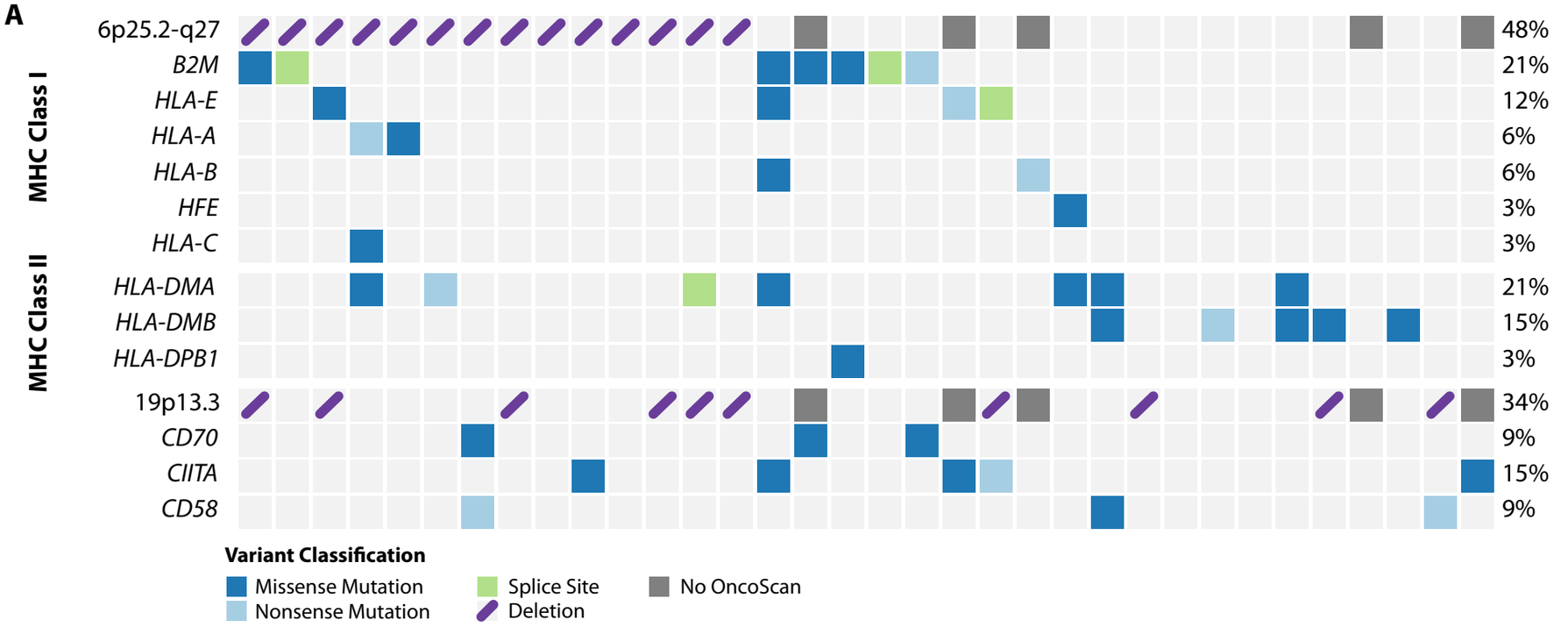
A
MHC Class I
MHC Class II
6p25.2-q27
B2M
HLA-E
HLA-A
HLA-B
HFE
HLA-C
HLA-DMA
HLA-DMB
HLA-DPB1
19p13.3
CD70
CIITA
CD58
48%
21%
12%
6%
6%
3%
3%
21%
15%
3%
34%
9%
15%
9%
Variant Classification
Missense Mutation
Nonsense Mutation
Splice Site
Deletion
No OncoScan

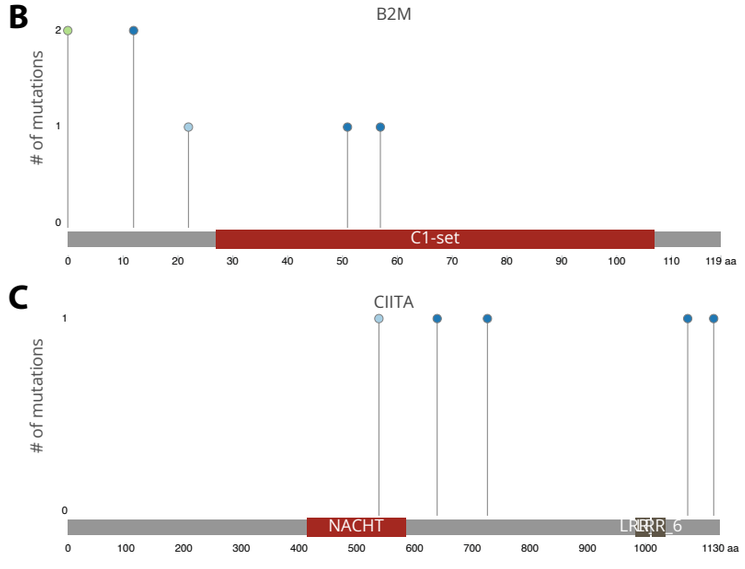
B
B2M
# of mutations
C1-set
119 aa
C
CIITA
# of mutations
NACHT
LRR
1130 aa

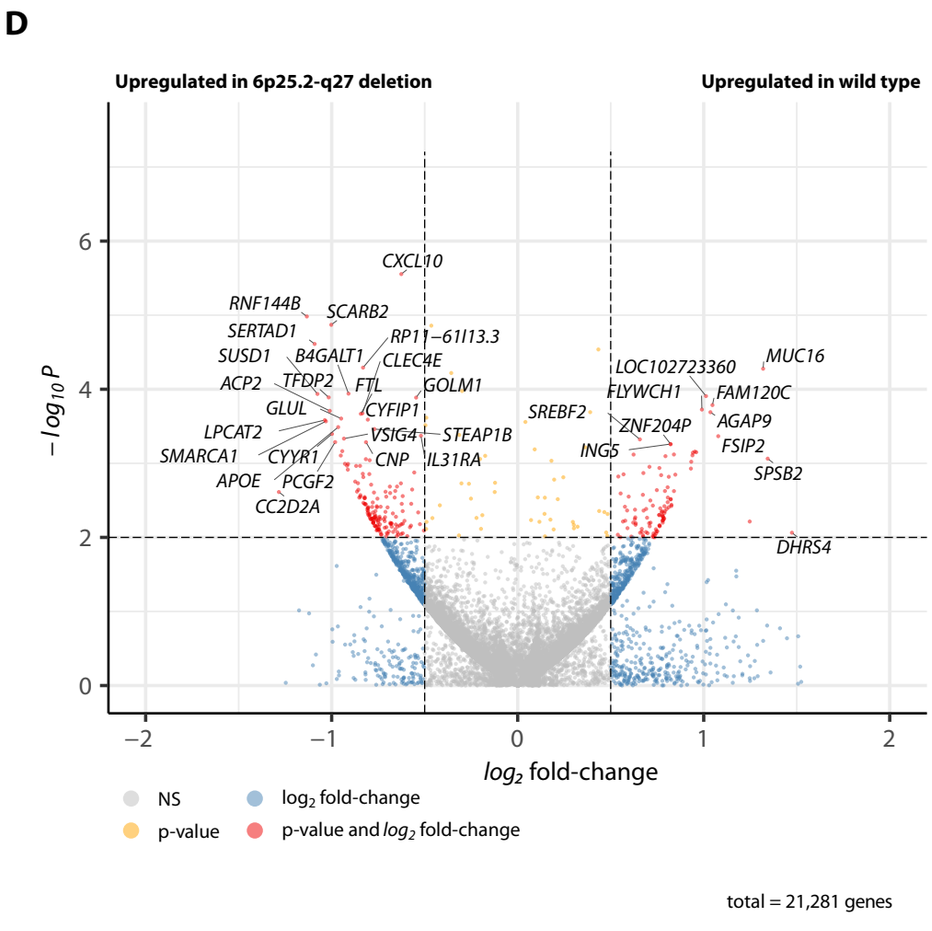
D
Upregulated in 6p25.2-q27 deletion
Upregulated in wild type
CXCL10
RNF144B
SCARB2
SERTAD1
RP11−61I13.3
SUSD1
B4GALT1
CLEC4E
ACP2
TFDP2
FTL
GOLM1
GLUL
CYFIP1
LPCAT2
VSIG4
STEAP1B
SMARCA1
CYYR1
CNP
IL31RA
APOE
PCGF2
CC2D2A
SREBF2
LOC102723360
MUC16
FLYWCH1
FAM120C
ZNF204P
AGAP9
ING5
FSIP2
SPSB2
DHRS4
−log10 P
log2 fold-change
NS
p-value
log2 fold-change
p-value and log2 fold-change
total = 21,281 genes

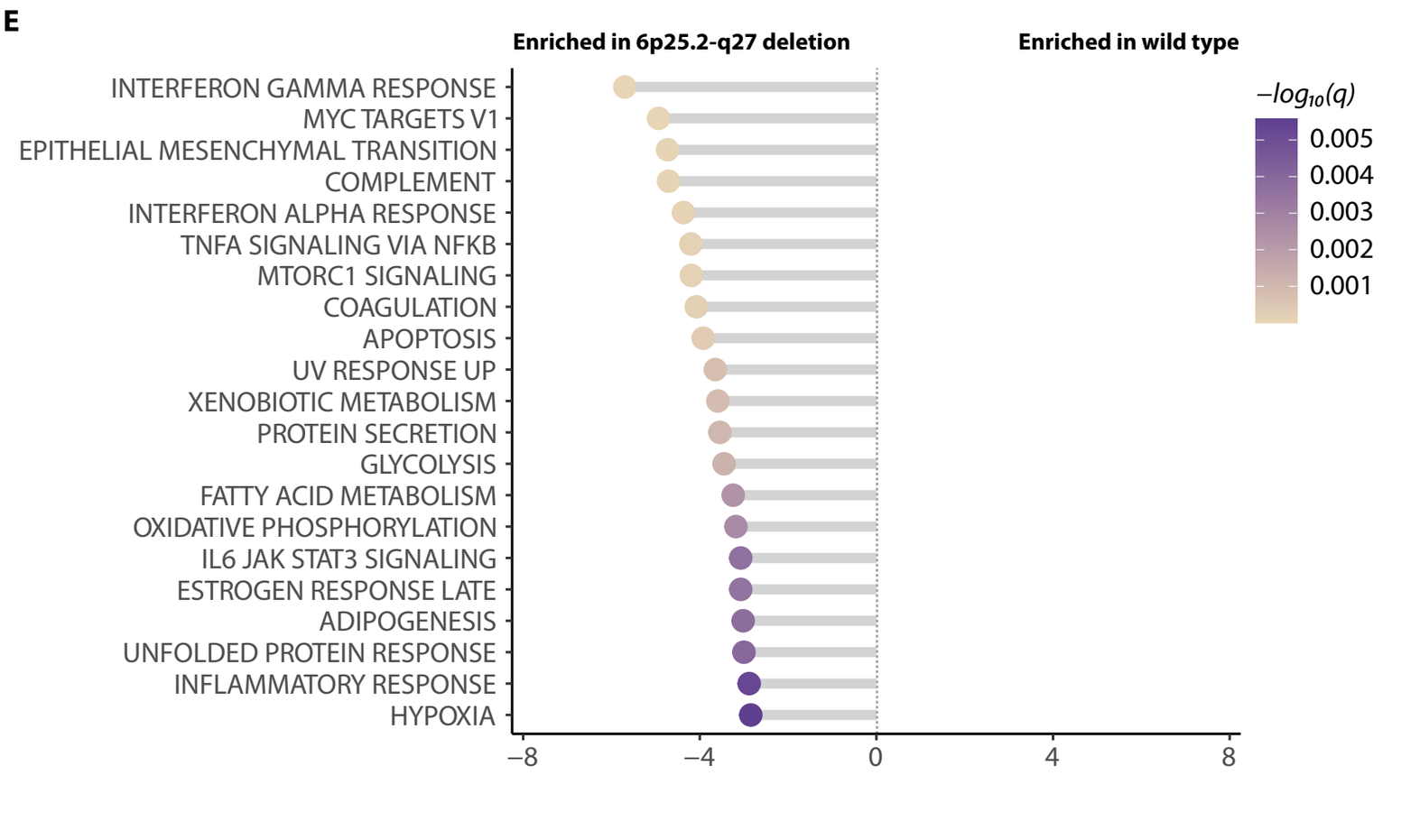
E
Enriched in 6p25.2-q27 deletion
Enriched in wild type
INTERFERON GAMMA RESPONSE
MYC TARGETS V1
EPITHELIAL MESENCHYMAL TRANSITION
COMPLEMENT
INTERFERON ALPHA RESPONSE
TNFA SIGNALING VIA NFKB
MTORC1 SIGNALING
COAGULATION
APOPTOSIS
UV RESPONSE UP
XENOBIOTIC METABOLISM
PROTEIN SECRETION
GLYCOLYSIS
FATTY ACID METABOLISM
OXIDATIVE PHOSPHORYLATION
IL6 JAK STAT3 SIGNALING
ESTROGEN RESPONSE LATE
ADIPOGENESIS
UNFOLDED PROTEIN RESPONSE
INFLAMMATORY RESPONSE
HYPOXIA
−log10(q)
0.005
0.004
0.003
0.002
0.001

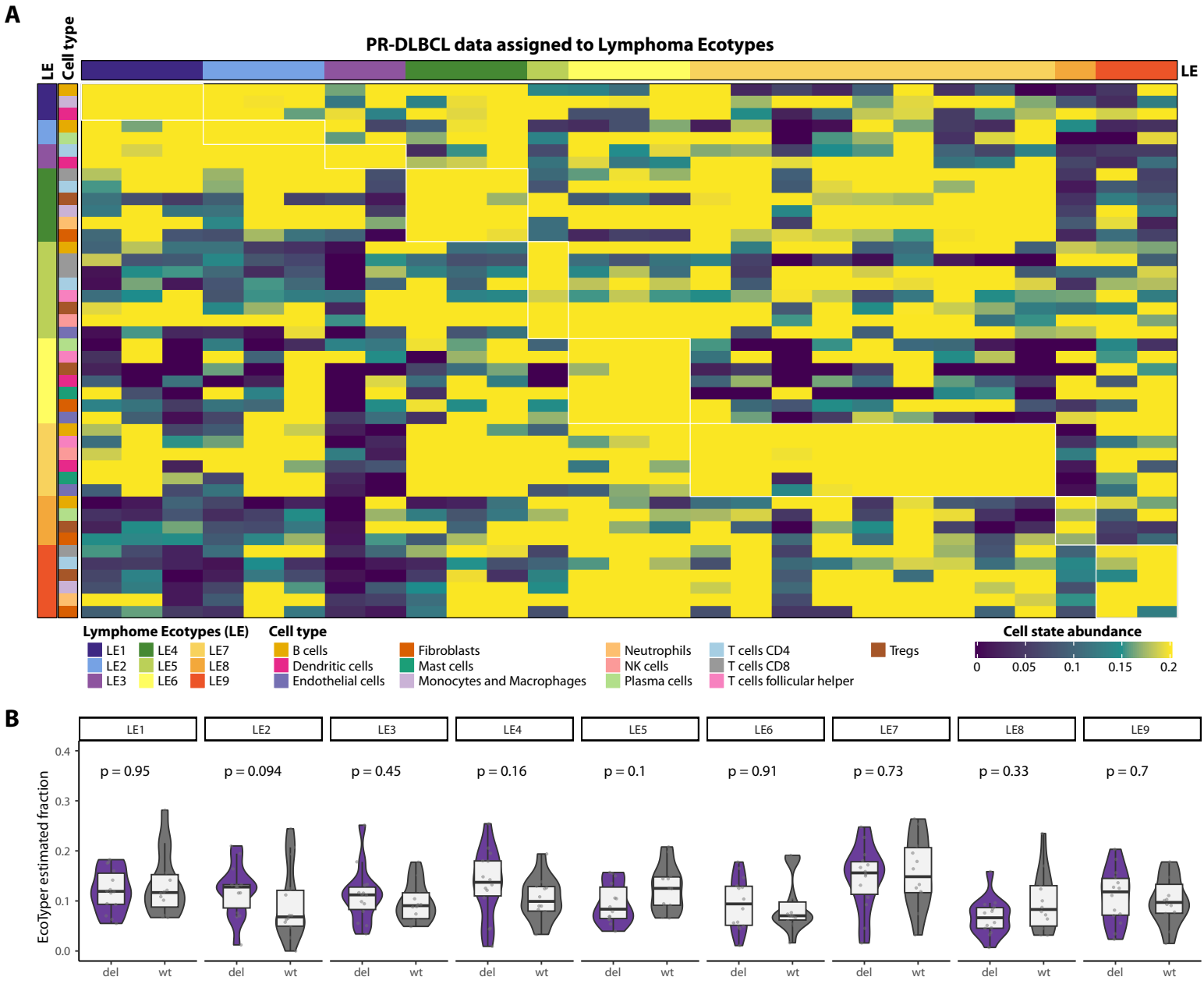
A
PR-DLBCL data assigned to Lymphoma Ecotypes
LE
Cell type
LE
Lymphome Ecotypes (LE)
LE1
LE2
LE3
LE4
LE5
LE6
LE7
LE8
LE9
Cell type
B cells
Dendritic cells
Endothelial cells
Fibroblasts
Mast cells
Monocytes and Macrophages
Neutrophils
NK cells
Plasma cells
T cells CD4
T cells CD8
T cells follicular helper
Tregs
Cell state abundance
0
0.05
0.1
0.15
0.2
B
LE1
LE2
LE3
LE4
LE5
LE6
LE7
LE8
LE9
p = 0.95
p = 0.094
p = 0.45
p = 0.16
p = 0.1
p = 0.91
p = 0.73
p = 0.33
p = 0.7
EcoTyper estimated fraction
0.0
0.1
0.2
0.3
0.4
del
wt